Engineering Cooperativity in Biomotor-Protein Assemblies

Michael R. Diehl,[1]*† Kechun Zhang,[1] Heun Jin Lee,[2] David A. Tirrell[1]

A biosynthetic approach was developed to control and probe cooperativity in multiunit biomotor assemblies by linking molecular motors to artificial protein scaffolds. This approach provides precise control over spatial and elastic coupling between motors. Cooperative interactions between monomeric kinesin-1 motors attached to protein scaffolds enhance hydrolysis activity and microtubule gliding velocity. However, these interactions are not influenced by changes in the elastic properties of the scaffold, distinguishing multimotor transport from that powered by unorganized monomeric motors. These results highlight the role of supramolecular architecture in determining mechanisms of collective transport.

Protein cooperativity allows systems of biomotor assemblies to operate with greater determinism and efficiency and often provides physiological functionality that cannot be achieved by single molecules (*1*–*9*). For example, cooperation between RNA polymerase molecules can result in increased rates of transcription (*2*), and increased transport velocities have been observed with groups of monomeric kinesin motors (*3*, *4*) and with multimotor assemblies comprising dimeric kinesins and dyneins (*5*). In the latter case, assemblies traveled in vivo with velocities up to 10 times as high as those observed in vitro. This result implies the presence of intermotor interactions in vivo that are not reproduced in in vitro assays. Although models of biomotor cooperativity (*1*, *6*) can explain generic aspects of multimotor transport and predict new modes of transport such as spontaneous oscillations (*7*–*11*), the molecular details that give rise to these cooperative effects remain elusive.

Many systems of motors are arranged in highly organized and hierarchical architectures in vivo (*12*, *13*), but it is not clear how features such as the mechanical compliance of motor-motor linkages and intermotor spacing influence collective dynamics. Because the mechanochemistry of biomotors is strongly dependent on strain [and hence on the mechanical coupling between motors (*14*, *15*)], developing a more complete picture of collective motility requires a better understanding of the relations between architecture and function in multimotor assemblies.

To investigate the influence of supramolecular architecture on biomotor cooperativity, we have engineered a model multimotor system that allows us to precisely regulate intermotor coupling. We have synthesized a series of modular polymeric scaffolds (Fig. 1) in which molecular properties such as length, sequence, and secondary structure are specified by artificial genes that encode alternating rigid and elastic protein motifs (*16*). The rigid block is comprised of strongly associated acidic and basic leucine zipper domains that anchor motor proteins at specific distances along the polymer backbone. Based on amino acid sequences developed by Vinson *et al.* (*17*), these zippers form strong heterodimeric complexes ($K_D \sim 10^{-15}$ M) and much weaker homodimers ($K_D \sim 10^{-6}$ to 10^{-3} M). The artificial protein scaffolds incorporate the basic zipper (Z_R) into the polymer backbone, whereas the complementary acidic zipper (Z_E) is fused to the C terminus of a truncated kinesin-1 motor (designated K350-Z_E). The flexible polymer block is derived from the elastomeric poly(VPGV$_\alpha$G) structural motif of the protein elastin (EL) and confers well-characterized mechanical compliance on the assembly (*18*–*20*). Every fifth α-valine (V_α) residue is replaced by a phenylalanine (F) residue in the EL sequence used here, yielding the designation ELF. This substitution provides a means to control the thermoresponsive behavior of the polymers, as discussed in more detail below. Variation in the number of diblock repeats in the polymer provides discrete control over the number of coupled motors, which in the present series of experiments ranges from one to three. The C terminus of each scaffold is labeled with biotin to allow the motor assemblies to be tethered to streptavidin-coated surfaces.

The monomeric kinesin-1 construct contains a Z_E-fusion to the motor's catalytic domain and neck linker. Monomeric truncations of kinesin-1 that contain the neck linker are nonprocessive

[1]Division of Chemistry and Chemical Engineering, California Institute of Technology, Pasadena, CA 91125, USA. [2]Department of Applied Physics, California Institute of Technology, Pasadena, CA 91125, USA.

*Present address: Department of Bioengineering and Department of Chemistry, Rice University, Houston, TX.
†To whom correspondence should be addressed. E-mail: diehl@rice.edu

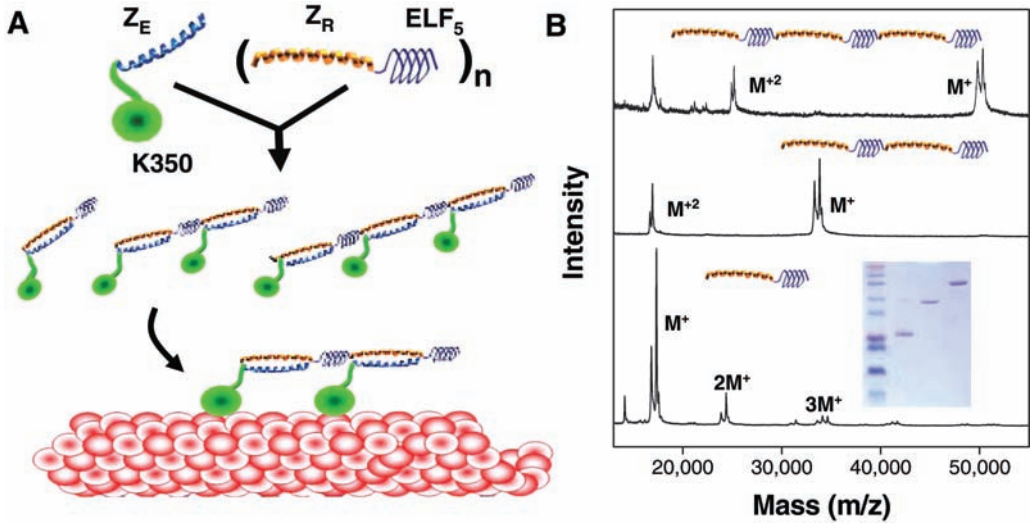

Fig. 1. Engineered multimotor assemblies. (**A**) Schematic representation of the synthesis of the engineered multimotor assemblies. As a complex, the zippers (Z_E and Z_R) form a rigid linker approximately 6.5-nm long (assuming 6.3 heptad repeats in a zipper and 1.03 nm per heptad) (*31*). The length of the flexible ELF block can be approximated by assuming a β-spiral conformation. In this conformational state, elastin proteins possess a spiral pitch of 1 nm, where each turn contains three VPGV$_\alpha$G pentapeptide units. Repeating this ELF motif, $(VPGVG)_2VPGFG(VPGVG)_2$, five times gives a length of 8 nm for the ELF_5 domain. Considering that four amino acids (KASK) form linkers between adjacent Z_R-ELF_5 diblock units, the total intermotor spacing set by the polymer is approximately 16 nm when bound to a microtubule (shown in red). (**B**) Matrix-assisted laser desorption/ionization mass spectra of polymer scaffolds containing one, two, and three repeats of the Z_R-ELF_5 diblock. The splitting of the main peaks (M+) is due to a 525-Da shift in mass that arises from biotin functionalization at the C-terminal cysteine positions of the polymers. A tris-tricine gel of all three polymers is shown in the inset.

and maintain plus-end directionality (*21*). As a result, the motions of individual K350-Z_E motors along microtubules can be described by Brownian diffusion models (*22*, *23*). When anchored to the Z_R blocks of the artificial protein scaffolds $(Z_R\text{-}ELF_5)_n$, motors are separated by approximately 16 nm, or two microtubule lattice sites (Fig. 1).

To examine the consequences of clustering multiple motors, we measured the microtubule-stimulated adenosine triphosphatase (ATPase) rates of the polymer-motor complexes (Fig. 2A). Motor assemblies were preformed in solution by incubating the $(Z_R\text{-}ELF_5)_n$ polymers and K350-Z_E motors (*16*, *24*). When assembled on dimeric $(Z_R\text{-}ELF_5)_2$ and trimeric $(Z_R\text{-}ELF_5)_3$ scaffolds, the K350-Z_E motors exhibit roughly a 60% increase in the maximum microtubule-stimulated ATPase rate (k_{cat}) accompanied by a decrease by a factor of 2.6 to 3.1 in the Michaelis-Menten constant ($K_{0.5MT}$) when compared with complexes formed on monomeric (Z_R-ELF_5) scaffolds (Fig. 2). Similar results were obtained by using either microtubule affinity–purified or Ni-NTA (nickel nitrilotriacetic acid)–purified K350-Z_E motors (Table 1).

Whereas the apparent bimolecular reaction rate ($k_{cat}/K_{0.5MT}$) of the monomeric motor complex falls within values predicted for diffusion-limited reactions (20 to 30 $\mu M^{-1}\ s^{-1}$) (*25*), the dimeric and trimeric complexes exhibit an increase by a factor of 4 or more in $k_{cat}/K_{0.5MT}$. This result suggests that the multiprotein complexes are processive. However, $k_{cat}/K_{0.5MT}$ values are smaller than those of native kinesin ($\geq$1000 $\mu M^{-1}\ s^{-1}$) (*26*), implying (as expected) a distinct transport mechanism.

In microtubule gliding assays (*16*), microtubule velocities of two- and three-headed multimotors are about twice that of the monomer constructs (Fig. 2B). In these experiments, polymer and motor concentrations were chosen to ensure that the coverslip surface was saturated with motor assemblies. In each case, microtubules exhibited smooth gliding motions across the surface. Thus, microtubule gliding is occurring in a regime where transport is characterized by multiprotein suppression of individual motor fluctuations and is independent of the number of motors involved in motility (*6*, *27*). As a result, multimotor complexes must use an additional mechanism that enhances the velocity-determining step of the K350-Z_E motors. This mechanism should be linked to the enhanced ATPase activity observed in solution phase experiments and is likely the result of specific motor-motor coupling that occurs when several motors are anchored along a single polymer chain. Interestingly, trimeric multimotor complexes produced gliding velocities similar to those of dimeric assemblies.

Insight into the nature of the intermotor coupling in the multimotor assemblies can be gained by tuning the elastic properties of the scaffold's ELF motif. Elastin-like polypeptides (ELPs) undergo a phase transition in which hydrophobic folding of the chain drives a condensation process, forming a denser viscoelastic phase when the temperature is raised above the lower critical solution temperature (LCST) of the protein (*18*). Single-molecule atomic force micoscopy pulling experiments demonstrate that the LCST transition results in a decrease in polymer length (*28*).

In concentrated polymer solutions, the condensation of ELPs can be monitored by measuring changes in turbidity with temperature (Fig. 3A). The transition temperature of the polymers increases with decreasing polymer length (*29*). In temperature-dependent microtubule gliding assays (Fig. 3B) (*16*), elastin condensation results in a decreased microtubule velocity. Similar behavior is observed when a stoichometric excess of the $(Z_R\text{-}ELF_5)_2$ polymer is used to produce longer monomeric motors. In each case, the microtubule gliding velocity increases with increasing temperature in accordance with a standard Arrhenius-like temperature dependence above and below the transition. However, the condensation of the ELF units is accompanied by a decrease in the slope, yielding 20 to 30% lower activation barriers above the LCST (Table 1).

The attenuation of microtubule velocity upon condensation of the ELF domains when transport is powered by monomeric complexes can be explained by previous models of cooperating motors. These models predict enhancements of multimotor efficiency, velocity, and force generation when motor anchorages are stiff (*1*, *3*). The observed decreases in both the velocities and activation barriers of micro-

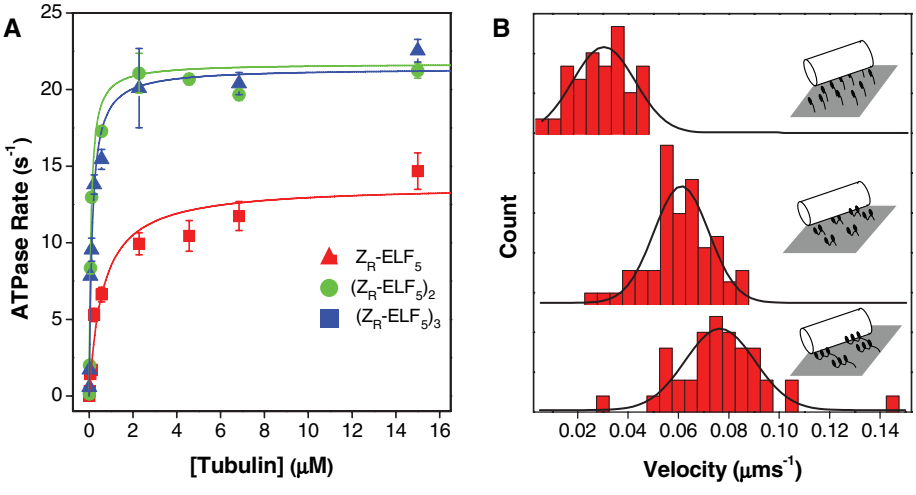

Fig. 2. Enhancement of ATPase activity and motility when multiple K350-Z_E motors are coupled to $(Z_R\text{-}ELF_5)_n$ polymer scaffolds. (**A**) Microtubule-dependent ATPase activity of $[K350\text{-}Z_E]_n/(Z_R\text{-}ELF_5)_n$ assemblies. The multimotor assemblies, $[K350\text{-}Z_E]_2/(Z_R\text{-}ELF_5)_2$ and $[K350\text{-}Z_E]_3/(Z_R\text{-}ELF_5)_3$, exhibit a 52% to 67% increase in the maximum ATPase rate (k_{cat}) compared with $[K350\text{-}Z_E]/(Z_R\text{-}ELF_5)$. The lines are Michaelis-Menten fits yielding $K_{0.5MT}$ (0.62 ± 0.20; 0.08 ± 0.01; 0.14 ± 0.20) and k_{cat} (13.7 ± 1.0; 21.7 ± 0.8; 21.4 ± 0.7) values for the monomer, dimer, and trimer complexes, respectively. (**B**) Velocity histograms for microtubules gliding over films prepared using preassembled motor/polymer complexes at 17°C for monomeric (top), dimeric (middle), and trimeric (bottom) complexes.

Table 1. Summary of kinetics and temperature-dependent gliding assays.

Assembly	MT Affinity-purified K350-Z_E			Ni-NTA purified K350-Z_E		
	$K_{0.5MT}$* (μM)	k_{cat}* (s^{-1})	$k_{cat}/K_{0.5MT}$* ($\mu M^{-1}\ s^{-1}$)	V† (nm s^{-1})	ΔE (T < TC) (kJ mol^{-1})	ΔE (T > TC) (kJ mol^{-1})
$[K350\text{-}Z_E]/(Z_R\text{-}ELF_5)$	0.75 ± 0.30	15.4 ± 2.3	20	29 ± 22	150	105
$[K350\text{-}Z_E]/(Z_R\text{-}ELF_5)_2$‡	—	—	—	—	163	133
$[K350\text{-}Z_E]_2/(Z_R\text{-}ELF_5)_2$	0.29 ± 0.08	23.4 ± 1.7	81	61 ± 22	——58——	
$[K350\text{-}Z_E]_3/(Z_R\text{-}ELF_5)_3$	0.24 ± 0.04	25.7 ± 0.9	104	76 ± 27	——69——	

*Measured at 20°C †MT gliding at 17°C ‡Monomeric complex using dimeric polymer

tubule transport are consistent with these theories if the simultaneous decrease in ELF length and stiffening of the mechanical linkage to the cover slip are taken into account. In microtubule gliding assays, the decrease in polymer length influences transport by producing a monomeric motor with a shorter "lever arm" and, consequently, a smaller working stroke.

Multimotor assemblies consisting of fully functionalized dimeric $[K350Z_E]_2/(Z_R\text{-}ELF_5)_2$ and trimeric $[K350\text{-}Z_E]_3/(Z_R\text{-}ELF_5)_3$ complexes exhibit simple Arrhenius-like temperature dependence throughout the ELF phase transition region (Fig. 3C). The activation barriers obtained from these measurements are substantially lower than those of the monomeric motor assemblies (Table 1). Here, the insensitivity of multimotor transport to ELF condensation suggests a mechanism that relies on processes distinct from those that dominate transport driven by teams of unorganized monomeric complexes. One explanation for the difference is that mechanochemical coupling between neighboring motors is enhanced by the stiffening of the ELF linkages, compensating for a decrease in motor working distance. However, this possibility requires that these two competing factors are in near-perfect balance for both dimeric and trimeric assemblies. Alternatively, the velocity determining step of multimotor transport may not be dependent on the motions of lever arms that contain the ELF linkers as structural elements. Instead, engineered assemblies may use a multistep mechanism that is rate-limited by other mechanical processes, such as motions where the motor's neck linkers alone serve as lever arms or a diffusive search by a motor domain for its next binding site.

Although models involving diffusion-to-capture processes and/or conformational changes in neck linkers have been used to describe the stepping mechanics of kinesins (*30*), the results reported here indicate that the artificial proteins provide a structural framework that allows motors to push and pull on one another to enhance activity. Such cooperative interactions should lead to "inchworm-like" stepping motions that are influenced by weak mechanochemical coupling and, possibly, by coordinated displacements along the microtubule. The mechanism of movement should be influenced by architectural features of the assembly, including the large intermotor distance, the flexibility of the ELF linkages, the ability of an assembly to bind multiple microtubule sites, and the asymmetric anchoring to the surface at one end of the scaffold. These features create a structural framework where motors are attached to the microtubule and to the surface through different mechanical linkages and where strain is unequally distributed across the motors in an assembly. These factors should constrain the mechanism of multimotor transport by determining the local reference frame for the displacement of a motor within an assembly and should influence cooperative interactions by tuning both the strain-dependent detachment of, and the mechanochemical coupling between, neighboring motors. Although further experiments to investigate the details of multimotor transport are underway, the results described here clearly demonstrate that controlling the supramolecular architecture of multimotor assemblies provides a means to reconfigure mechanisms of collective biomotor transport.

References and Notes

1. F. Julicher, A. Ajdari, J. Prost, *Rev. Mod. Phys.* **69**, 1269 (1997).
2. V. Epshtein, E. Nudler, *Science* **300**, 801 (2003).
3. Y. Okada, N. Hirokowa, *Nature* **424**, 574 (2003).

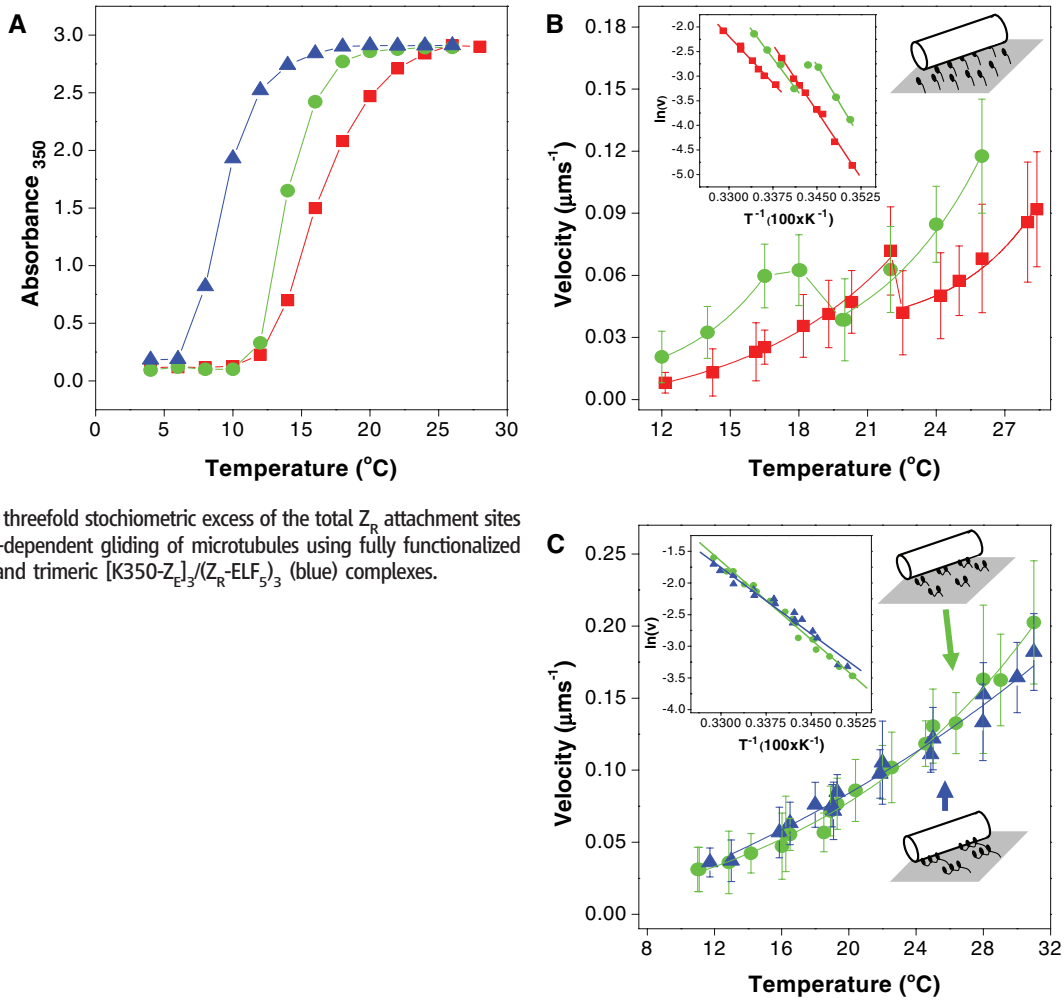

Fig. 3. Influence of the condensation of the ELF domain of the polymers on multimotor motility. (**A**) Solution-phase LCST behavior of $[Z_E]_n/(Z_R\text{-}ELF_5)_n$ complexes measured in motility buffer (at equal $Z_R\text{-}ELF_5$ concentration: 2 mM). Condensation of the ELF domain produces an increase in turbidity of the solution as the temperature rises. (**B**) and (**C**) Temperature-dependent microtubule gliding velocities of monomeric (B) and multimeric (C) polymer/motor complexes. (B) Monomeric complexes were formed using either the $Z_R\text{-}ELF_5$ (red) or the dimeric $(Z_R\text{-}ELF_5)_2$ (green) polymers. Monomeric assemblies were prepared from the dimeric $(Z_R\text{-}ELF_5)_2$ polymers by using a threefold stochiometric excess of the total Z_R attachment sites relative to the motor. (C) Temperature-dependent gliding of microtubules using fully functionalized dimeric $[K350\text{-}Z_E]_2/(Z_R\text{-}ELF_5)_2$ (green) and trimeric $[K350\text{-}Z_E]_3/(Z_R\text{-}ELF_5)_3$ (blue) complexes.

4. D. R. Klopfenstein, M. Tomishige, N. Stuurman, R. D. Vale, *Cell* **109**, 347 (2002).
5. C. Kural *et al.*, *Science* **308**, 1469 (2005).
6. S. Leibler, D. A. Huse, *J. Cell Biol.* **121**, 1357 (1993).
7. S. A. Endow, H. Higuchi, *Nature* **406**, 913 (2000).
8. M. Badoual, F. Julicher, J. Prost, *Proc. Natl. Acad. Sci. U.S.A.* **99**, 6696 (2002).
9. F. Jülicher, J. Prost, *Phys. Rev. Lett.* **78**, 4510 (1997).
10. S. Camalet, F. Julicher, J. Prost, *J. Phys. Rev. Lett.* **82**, 1590 (1999).
11. S. Camalet, T. Duke, F. Julicher, J. Prost, *Proc. Natl. Acad. Sci. U.S.A.* **97**, 3183 (2000).
12. S. A. Burgess, *J. Mol. Biol.* **250**, 52 (1995).
13. S. P. Gross, Y. Guo, J. E. Martinez, M. A. Welte, *Curr. Biol.* **13**, 1660 (2003).
14. T. Duke, *Philos. Trans. R. Soc. Lond. B Biol. Sci.* **355**, 529 (2000).
15. A. Vilfan, E. Frey, F. Schwabl, *Eur. Phys. J. B* **3**, 535 (1998).
16. Materials and methods are available as supporting material on *Science* Online.
17. J. R. Moll, S. B. Ruvinov, I. Pastan, C. Vinson, *Protein Sci.* **10**, 649 (2001).
18. D. W. Urry, *J. Phys. Chem. B* **101**, 11007 (1997).
19. D. W. Urry *et al.*, *Philos. Trans. R. Soc. Lond. B Biol. Sci.* **357**, 169 (2002).
20. Polymer flexibility can be estimated by calculating the elastic spring constant (κ) of a single ELF_5 linker using data from single molecule force-extension measurements. These experiments yield persistence lengths (L_p) for elastins of $\sim$ 0.4 nm in the low force regime. Assuming a wormlike chain model for the polymer at low extension, κ can be estimated from $\kappa = 3k_bT/2L_pL_c$, where L_c is the contour length of the polymer, k_b is the Boltzman constant, and T is temperature. A single ELF_5 linker contains $\sim$125 amino acids, yielding L_c = 36.35 nm, assuming 0.29 nm per residue, and κ = 0.4 pN/nm.
21. R. B. Case, D. W. Pierce, N. Hom-Booher, C. L. Hart, R. D. Vale, *Cell* **90**, 959 (1997).
22. Y. Inoue, A. H. Iwane, T. Miyai, E. Muto, T. Yanagida, *Biophys. J.* **81**, 2838 (2001).
23. Y. Okada, N. Hirokawa, *Science* **283**, 1152 (1999).
24. Polymer-motor assemblies were formed by making a master mix of K350-Z_E and $(Z_R\text{-}ELF_5)_n$ polymers and incubating for at least 20 min at 4°C before addition to the reaction. Concentrations of polymer solutions were determined from their A_{280} values, using an extinction coefficient of 1480 cm^{-1} mol^{-1} for each Z_R-ELF_5 repeat in the polymers. The fidelity of the assembly process was examined for the trimeric $[K350\text{-}Z_E]_3/(Z_R\text{-}ELF_5)_n$ complex using selectively radiolabeled proteins and multichannel scintillation counting. In these experiments, a K350-Z_E motor was radiolabeled with ^{35}S (77,104 cpm/nmol) by expressing the motor in 1 liter of LB medium supplemented with L-[^{35}S]cysteine (5 mCi). Similarly, a ^3H labeled $(Z_R\text{-}ELF_5)_3$ polymer (33,046 cpm/nmol) was prepared by expression in 0.1 L of LB medium supplemented with L-[3,4(n)-^{3}H]valine (2.5 mCi). After purification, the polymer was functionalized with a PEO-biotinmaleimide (Pierce) using standard maleimide labeling protocols. Then, radiolabeled polymers and motors were mixed in a 1:1.5 ratio with respect to the Z_R sites of the polymer and the motor. After incubation, the [motor]/(polymer) complex was selectively bound to a neutravidin resin. Excess motor was washed from the resin, and the sample, including the resin, was transferred to a scintillation vial. Comparison of the signals from ^{35}S and ^3H channels yielded a motor/polymer ratio of 2.9 $\pm$ 0.4. Control experiments were performed with the polymers omitted from solution; results indicated nonspecific binding of the K350-Z_E motors to the resin did not influence our measurements.
25. D. D. Hackney, *Biophys. J.* **68**, 267s (1995).
26. D. D. Hackney, *Nature* **377**, 448 (1995).
27. W. O. Hancock, J. Howard, *J. Cell Biol.* **140**, 1395 (1998).
28. J. Hyun, W.-K. Lee, N. Nath, A. Chilkoti, S. Zauscher, *J. Am. Chem. Soc.* **126**, 7330 (2004).
29. D. E. Meyer, A. Chilkoti, *Biomacromolecules* **5**, 846 (2004).
30. N. J. Carter, R. A. Cross, *Nature* **435**, 308 (2005).
31. F. H. C. Crick, *Acta Crystallogr.* **6**, 689 (1953).

32. We thank A. J. Link and I. Fushman their help during the early stages of this project; L. Wade and D. Pearson for use of the temperature controller; and P. Wiggins, R. Bao, T. Squires, and S. Quake for valuable discussions. This work was supported by the Beckman Foundation through a Beckman Senior Research Fellowship (to M.R.D.) and by a grant from the National Science Foundation.

Supporting Online Material

www.sciencemag.org/cgi/content/full/311/5766/1468/DC1
Materials and Methods
Table S1
References

2 November 2005; accepted 6 February 2006
10.1126/science.1122125

Progressive Disruption of Cellular Protein Folding in Models of Polyglutamine Diseases

Tali Gidalevitz,* Anat Ben-Zvi,* Kim H. Ho, Heather R. Brignull, Richard I. Morimoto†

Numerous human diseases are associated with the chronic expression of misfolded and aggregation-prone proteins. The expansion of polyglutamine residues in unrelated proteins is associated with the early onset of neurodegenerative disease. To understand how the presence of misfolded proteins leads to cellular dysfunction, we employed *Caenorhabditis elegans* polyglutamine aggregation models. Here, we find that polyglutamine expansions disrupted the global balance of protein folding quality control, resulting in the loss of function of diverse metastable proteins with destabilizing temperature-sensitive mutations. In turn, these proteins, although innocuous under normal physiological conditions, enhanced the aggregation of polyglutamine proteins. Thus, weak folding mutations throughout the genome can function as modifiers of polyglutamine phenotypes and toxicity.

Although many results from in vitro and in vivo models that express mutant Huntingtin, α-synuclein, tau, superoxide dismutase-1, amyloid-β peptide, or prion proteins are consistent with the proposal that non-native species can form toxic folding intermediates, oligomers, and aggregates (*1*–*5*), distinct mechanisms for toxicity have been proposed for each. These mechanisms range from specific protein-protein interactions to disruption of various cellular processes, including transcription (*6*, *7*), protein folding (*8*, *9*), protein clearance (*10*–*13*), energy metabolism (*14*), activation of apoptotic pathways (*15*), and others. This has led us to consider how the expression of a single aggregation-prone protein could have such pleiotropic effects and whether a more general mechanism could explain the many common features of protein conformation diseases. Moreover, because each cell and tissue contains various metastable polymorphic proteins (*16*), could the chronic expression of an aggregation-prone protein have global consequences on homeostasis and thus affect folding or stability of proteins that harbor folding defects?

To test this hypothesis, we took a genetic approach using diverse *Caenorhabditis elegans* temperature-sensitive (ts) mutations to examine whether the functionality of the respective protein at the permissive condition was affected by expression of aggregation-prone polyglutamine (polyQ) expansions. Because many ts mutant proteins are highly dependent on the cellular folding environment (*17*–*19*), they represent highly sensitive indicators of a disruption in protein homeostasis. We employed transgenic *C. elegans* lines expressing different-length polyQ-YFP (yellow fluorescent protein) or CFP (cyan fluorescent protein) from integrated arrays in muscle (polyQm) (*20*, *21*) or neuronal (polyQn) (*22*) cells. Both models show polyQ-length–dependent aggregation and toxicity.

Animals expressing ts mutant UNC-15 (*C. elegans* homolog of a muscle paramyosin) were crossed to *C. elegans* polyQm strains, and phenotypes at permissive and restrictive conditions were examined in double homozygotes. At the restrictive temperature, this ts mutation disrupts thick filament formation and leads to embryonic and early larval lethality and slow movement in adults (*23*). Expression of polyQ proteins alone in a wild-type background did not result in these embryonic and larval phenotypes. In contrast, more than 40% of embryos coexpressing mutant paramyosin and Q40m [paramyosin(ts)+Q40m] failed to hatch or

Department of Biochemistry, Molecular Biology, and Cell Biology, Rice Institute for Biomedical Research, Northwestern University, Evanston, IL 60208, USA.

*These authors contributed equally to this work.
†To whom correspondence should be addressed. E-mail: r-morimoto@northwestern.edu